Available online at www.sciencedirect.com
SCIENCE DIRECT
Trans. Nonferrous Met. Soc. China 18(2008) 383−387
Transactions of Nonferrous Metals Society of China
www.csu.edu.cn/ysxb/

# New fracture morphology of amorphous $Fe_{78}Si_9B_{13}$ alloy

ZHANG Kai-feng(张凯锋), LI Xi-feng(李细锋)

School of Materials Science and Engineering, Harbin Institute of Technology, Harbin150001, China

Received 29 March 2007; accepted 24 July 2007

**Abstract:** The tensile fracture morphology of a brittle amorphous Fe-based ribbon was investigated by scanning electron microscopy(SEM). The fracture surface consists of mirror, mist and river-pattern zones with crack propagating. The formation of nanoscale damage cavity structure is a main characteristic morphology on the fracture surface. Approaching the fracture source in the mirror, these damage cavities assemble and form the nanoscale periodic striation patterns, which are neither Wallner lines nor crack front waves. At shear deformation stage, the apparent surface energy $\gamma_f$ of amorphous $Fe_{78}Si_9B_{13}$ ribbon is much smaller than that of less-brittle amorphous alloys, which indirectly indicates amorphous $Fe_{78}Si_9B_{13}$ ribbon is perfectly brittle. The crack branching appears at the moment of final fracture due to the high crack propagating velocity.

**Key words:** amorphous $Fe_{78}Si_9B_{13}$ alloy; damage cavity; periodic striation pattern

## 1 Introduction

Despite the physical process of catastrophic shear and ductile failure in amorphous ribbons has been studied for many years[1−2], the exact deformation and fracture mechanism of amorphous alloys remain unclear compared with those of crystalline materials. In general, the plastic deformation of amorphous alloys is localized in the narrow shear bands, followed by the rapid propagation of these shear bands and catastrophic fracture[3−5]. The tensile fracture characteristics of bulk metallic glasses(BMGs) have been extensively investigated in the last two decades. It was generally thought that fracture morphologies of BMGs are more complicated than those of amorphous alloy ribbons. However, WANG et al[6] recently observed the periodic morphology evolution on fracture surface of a brittle amorphous $Fe_{73.5}Cu_1Nb_3Si_{13.5}B_9$ alloy ribbon. The nanoscale swirling periodic corrugation patterns were formed by the self-assembly of the nanoscale damage cavities on the fracture surface. Thus further observations and analysis of fracture morphologies in amorphous alloy ribbons should be of special importance and great value.

In the present work, the tensile fracture morphologies of amorphous $Fe_{78}Si_9B_{13}$ ribbon were investigated by scanning electron microscopy(SEM). New fracture features have been found and fracture mechanisms were discussed based on the experimental observations.

## 2 Experimental

The amorphous $Fe_{78}Si_9B_{13}$ ribbon with a size of 30 μm in thickness and 20 mm in width, prepared by melt spinning, was supplied by the National Amorphous Nanocrystalline Alloy Engineering Research Center of China. X-ray diffraction confirmed that the ribbons used in this work were amorphous in the as-received state. Uniaxial tensile tests at room temperature along the length direction were performed on an Instron-CSS88000 machine with an initial strain rate of $8.33\times10^{-4}\ s^{-1}$. The tensile specimens were obtained by wire electrical discharge machining with a gauge of 10 mm in length and 3 mm in width. The fracture surfaces of the specimens after tension were observed using a HITACHI S-4700 scanning electron microscope (SEM) with spatial resolution of 1.5 nm.

## 3 Results and discussion

The nominal tensile stress—strain curve of amorphous $Fe_{78}Si_9B_{13}$ alloy ribbon is shown in Fig.1(a).

**Corresponding author:** LI Xi-feng; Tel: +86-451-86413681; E-mail: lixifeng0110@hit.edu.cn, lixifeng0110@163.com

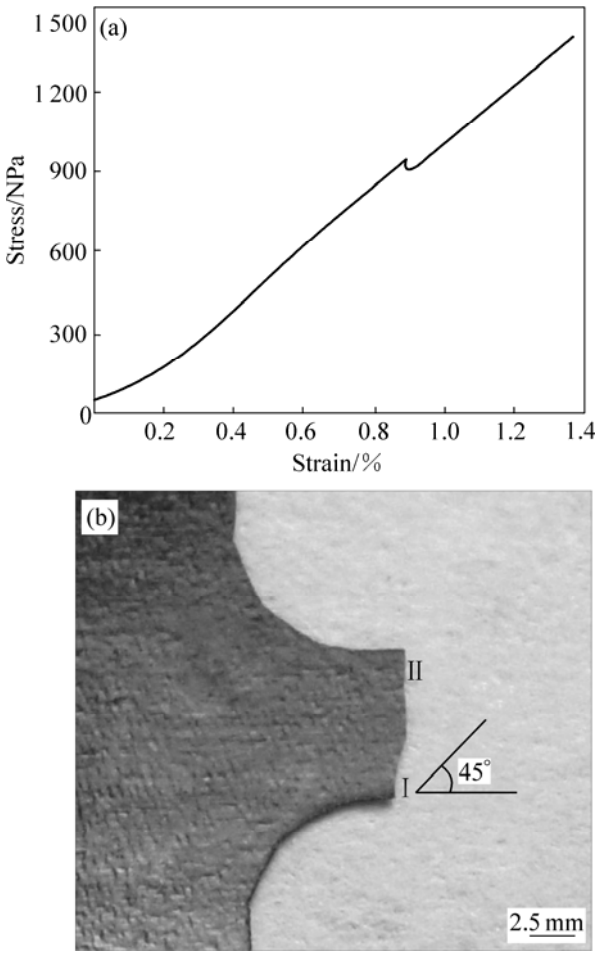


**Fig.1** Tensile characteristics of amorphous $Fe_{78}Si_9B_{13}$ ribbon: (a) Nominal stress—strain curve; (b) Side view of fracture specimen with sketch of angle

The curve exhibits a nearly linear relation. It is clearly seen that the amorphous ribbon deforms elastically and fractures immediately after yielding. This indicates that amorphous $Fe_{78}Si_9B_{13}$ alloy is an ideally brittle metallic glass at room temperature. Fig.1(b) shows the side looking of the fractured specimens with a sketch of the fracture angle. The fracture of amorphous ribbon takes place deviated from the maximum shear plane, which is declined by about 65° to the direction of the tensile load. This is the reason that the normal stress applied on the shear plane is very high and plays an important role in the fracture process of amorphous ribbon. This result is consistent with previous findings and theoretical analysis [5,7−8]. According to ZHANG et al[7−8], the tensile shear fracture angel $\theta_t$ of metallic glasses can be expressed as

$$\theta_t = \arctan\left(\sqrt{1+(\mu_t)^2}+\mu_t\right) > 45^\circ \quad (1)$$

where $\mu_t=\tau_0/\sigma_0$, $\tau_0$ is critical shear fracture stress without normal stress and $\sigma_0$ is critical normal fracture stress without shear stress. Eqn.(1) also indicates that the normal stress must be considered during the fracture of metallic glasses and tensile angles can be larger than 45°. It is supposed that the specimens fracture initially not in a pure shear mode (region Ⅰ) and end up with a hysterical fracture (region Ⅱ).

Fig.2 shows that a periodic striation pattern in the mirror zone (region I) is near to the fracture source. Spacing or wavelength of the densely packed striation pattern is about 150 nm and roughness of the striated surface is estimated to be about decades of nanometers. The wavelength of periodic striation in amorphous $Fe_{78}Si_9B_{13}$ ribbon is much larger than that in brittle $Mg_{65}Cu_{15}Ni_5Gd_{10}$ BMG (~50 nm)[9], less-brittle $Ni_{42}Cu_5Ti_{20}Zr_{21.5}Al_8Si_{3.5}$ BMG (~60 nm)[10], brittle $Fe_{73.5}Cu_1Nb_3Si_{13.5}B_9$ glassy ribbon (~70 nm)[6], and brittle $Mg_{65}Cu_{25}Tb_{10}$ BMG (~100 nm)[11]. This indicates that the wavelength size of the striations on the fracture surface is determined by the principal factors such as loading modes, material composition and mechanical properties. Striation structures with different orientations may co-exist, in which two striations encounter. The dashed line shows the border of the two structures, whose width is about decades to hundreds of nanometers. This means that structures with different orientations can hardly be superposed together.

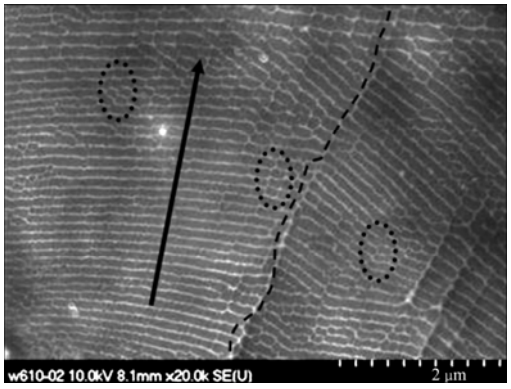


**Fig.2** SEM image showing periodic striation pattern in mirror zone near to crack origin (Arrow shows crack propagation direction)

The self-assembly of damage cavities along the fracture surface can clearly be observed on the marked areas also shown in Fig.2. The formation of damage cavity structure is a characteristic morphology in amorphous alloys[6,9,11]. Previous observations also demonstrate that a certain cavity density is required to form a periodic striation pattern. This indicates that self-assembly occurs only when damage cavities are

close enough and within each other's elastic influence range. The threshold of characteristic cavity size for periodic striation formation is estimated to be about 150 nm. Any theory describing the instability of fractograph must include the following two processes: the tendency to extend crack by means of viscous flow to release free energy, and the constraining effect impeding a fast crack growing by the formation of damage cavities ahead of the crack tip. When cavities accumulate along certain directions under certain stress field, extra energy dissipation of the fasting moving crack should be balanced with energy transfer along the dynamic steady-state crack front. Elastic waves generated from the fast running crack front as well as their reflected wave by the sample boundaries interfere with the stress fields of the crack tip. A complicated directional stress field is formed. This can decrease the size of the damage cavity and increase the density of cavities. The periodic striation patterns are formed by the combined result of the two processes.

During dynamic fracture of brittle amorphous materials, fracture energy will be released in the form of various elastic waves. Two kinds of elastic waves patterns, i.e., crack front wave and Wallner lines, have been observed in brittle soda-lime glasses[12−13]. It is thought that the striation patterns in the present study are different from Wallner lines by estimating the frequency of the crack propagation[13]. The frequency crack velocity oscillating in the brittle amorphous alloys is estimated to be in the order of $10^4$ MHz[11], far beyond the reasonable acoustic emission frequency range (1 kHz− 2 MHz). The corrugations are also not crack front waves as it is impossible to exist in periodic structural asperities in amorphous $Fe_{78}Si_9B_{13}$ ribbon with homogenous microstructure.

With crack propagating, the mirror zone is replaced by the mist zone. Fig.3 illustrates well-developed vein pattern in the mist zone (region Ⅰ). Veins patterns indicate

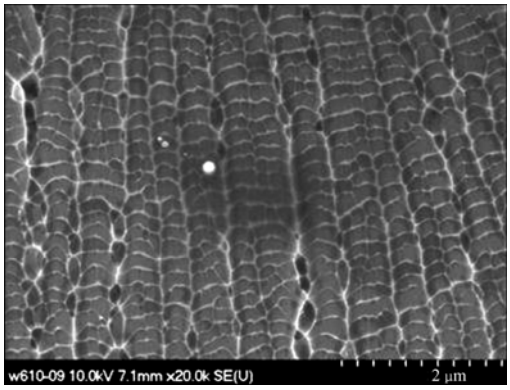


**Fig.3** SEM image showing vein morphology in mist zone (region Ⅰ)

a pre-melting state of amorphous alloys on the shear failure surfaces. But there is the absence of droplets and metal fibers that show evidence of a liquid phase. This is ascribed to the high melting temperature range (1 150− 1 165 ℃) of amorphous $Fe_{78}Si_9B_{13}$ alloy [14]. The cell-like vein pattern contains a number of damage cavities with size of about 250 nm. Its size is obviously larger than that in the mirror zone.

Compared with typical ductile amorphous $Ni_{78}Si_8B_{14}$ alloy ribbon and Zr-based BMG, the apparent surface energy $\gamma_f$ (which includes the work of plastic deformation) of amorphous materials during the cell-like veins pattern formation can be estimated by[15]

$$\gamma_f = 0.004\,06 \times \frac{\sigma_f}{N} \tag{2}$$

where $\sigma_f$ is the failure stress, and $N$ is the linear density, whose value is taken to be the inverse of cell diameter. In amorphous $Fe_{78}Si_9B_{13}$ ribbon, $\sigma_f$=1.39 GPa, $N$=1.5×$10^6$ $m^{-1}$, then $\gamma_f$=3.7 J/$m^2$. It can be seen that $\gamma_f$ of amorphous $Fe_{78}Si_9B_{13}$ ribbon is much smaller than that of ductile amorphous $Ni_{78}Si_8B_{14}$ alloy ribbon (28 J/$m^2$) and Zr-based BMG (97 J/$m^2$)[2]. The smaller work of plastic deformation during the vein-pattern formation in amorphous $Fe_{78}Si_9B_{13}$ ribbon is observed. This indirectly indicates that amorphous $Fe_{78}Si_9B_{13}$ ribbon is perfectly brittle.

In region II, the river patterns appear in the stage of failure end as shown in Fig.4(a). The river patterns are formed due to the crack branching that also generates numerous damage cavities. Fig.4 (b) shows their size of about 400 nm on the valley of crack branching. The crack branching is usually regarded as the result of the high crack propagating velocity. Such river-pattern zone is possibly dominated by the change of local stress intensity.

Fig.5 shows the schematic sketch of fracture surface morphology formed during the tensile test of amorphous $Fe_{78}Si_9B_{13}$ ribbon. It consists of mirror, mist, and river-pattern zones with crack propagating. Near to the fracture source, the crack propagation velocity is not high compared with that in river-pattern zone. The formation of nanoscale damage cavities demonstrates a blunted plane crack and the propagation of the fracture front via the coalescence of the damage cavities. The high tensile stress at the crack front can lead to the growth and coalescence of the cavities along the cavities along the crack surface. According to PAN et al[9], the periodic striation pattern becomes more unstable with the increase of load rate. Thus the velocity of crack propagation is high at the final fracture stage, and the fracture morphology transforms to river-pattern zone.

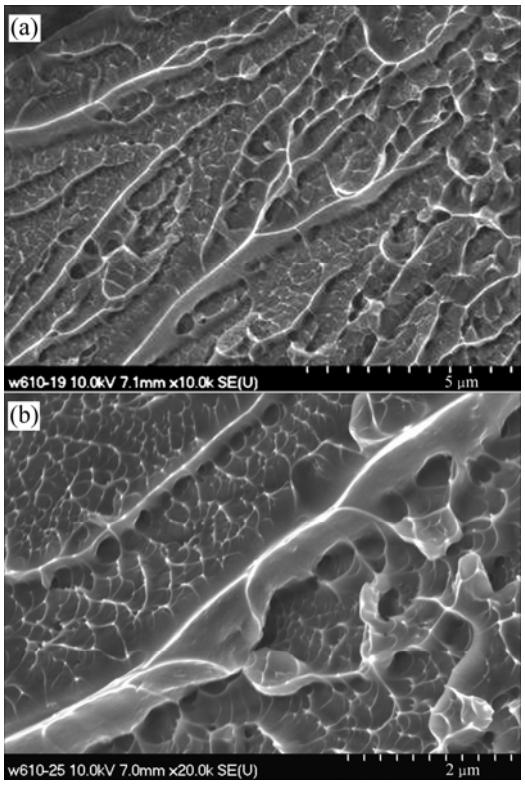


**Fig.4** SEM images showing crack branching in river-pattern zone: (a) Low magnification; (b) High magnification

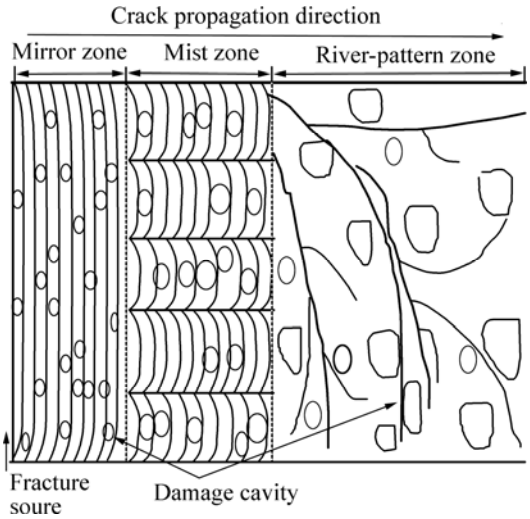


**Fig.5** Schematic sketch of fracture surface pattern formed during tensile test of amorphous $Fe_{78}Si_9B_{13}$ ribbon

There is a great variance between the stress fields of three zones, which leads to the size of nanoscale damage cavities increasing with crack propagation.

In this type of crack propagation, many damage cavities form rapidly at the crack tip and the material between the cavities necks down. Similar fracture experiments performed in other brittle metallic glasses such as Mg-based BMG and Ni-based BMG reveal a similar cavity structure, suggesting that the existence of damage cavities does not depend on the chemical composition and experimental conditions. This implies that there exists the universality to the dynamics during the dynamic fracture of brittle metallic glasses. The nucleation and coalescence of cavities relate to the glassy structure, which contains an amount of free volume and inherent atomic density fluctuation in the nanometer scale[16−17]. In fact, the lowest density zones behave as stress concentrators and grow under the stress imposed by the presence of the main crack to generate the damage cavities.

## 4 Conclusions

1) The fracture surface consists of mirror, mist and river-pattern zones with crack propagating. The formation of nanoscale damage cavity structure is a main characteristic morphology on the fracture surface due to the glassy structure that contains an amount of free volume and inherent atomic density fluctuation at the nanometer scale.

2) Approaching the fracture source in the mirror, these damage cavities assemble and form the nanoscale striation patterns, which are neither Wallner lines nor crack front waves.

3) At the shear deformation stage, the apparent surface energy $\gamma_f$ of amorphous $Fe_{78}Si_9B_{13}$ ribbon is 3.7 J/m$^2$, which is much smaller than $\gamma_f$ of less-brittle amorphous alloys.

4) The river-pattern zone appears at final fracture stage due to the high crack propagating velocity.

## References

[1] LEAMY H J, WANG T T, CHEN H S. Plastic flow and fracture of metallic glass (tensile plastic flow and fracture behavior of PdSi based alloys in glassy microcrystalline and crystalline states, noting shear deformation bands) [J]. Met Trans, 1972, 3: 699−708.

[2] BENGUS V Z, TABACHNIKOVA E D, MIŠKUF J, CSACH K, OCELÍK V, JOHNSON W L, MOLOKANOV V V. New features of the low temperature ductile shear failure observed in bulk amorphous alloys [J]. J Mater Sci, 2000, 35: 4449−4457.

[3] PAMPILLO C A. Flow and fracture in amorphous alloys [J]. J Mater Sci, 1975, 10: 1194−1227.

[4] INOUE A. Stabilization of metallic supercooled liquid and bulk amorphous alloys [J]. Acta Mater, 2000, 48: 279−306.

[5] ZHANG Z F, ECKERT J, SCHULTZ L. Difference in compressive and tensile fracture mechanisms of $Zr_{59}Cu_{20}Al_{10}Ni_8Ti_3$ bulk metallic glass [J]. Acta Mater, 2003, 51(4): 1167−1179.

[6] WANG G, WANG Y T, LIU Y H, PAN M X, ZHAO D Q, WANG W H. Evolution of nanoscale morphology on fracture surface of brittle metallic glass [J]. Appl Phys Lett, 2006, 89: 121909(1−3).

[7] ZHANG Z F, HE G, ECKERT J, SCHULTZ L. Fracture mechanisms in bulk metallic glassy materials [J]. Phys Rev Lett, 2003, 91(4):

045505(1−4).

[8] ZHANG Z F, ECKERT J. Unified tensile fracture criterion [J]. Phys Rev Lett, 2005, 94: 094301(1−4).

[9] PAN D G, ZHANG H F, WANG A M, WANG Z G, [J] HU Z Q. Fracture instability in brittle Mg-based bulk metallic glasses [J]. J Alloys Compd, 2007, 438(1/2): 145−149.

[10] SHEN J, LIANG W Z, SUN J F. Formation of nanowaves in compressive fracture of a less-brittle bulk metallic glass [J]. Appl Phys Lett, 2006, 89: 121908(1−3).

[11] XI X K, ZHAO D Q, PAN M X, WANG W H, WU Y, LEWANDOWSKI J J. Periodic corrugation on dynamic fracture surface in a brittle bulk metallic glass [J]. Appl Phys Lett, 2006, 89: 181911(1−3).

[12] SHARON E, COHEN G, FINEBERG J. Crack front waves and the dynamics of a rapidly moving crack [J]. Phys Rev Lett, 2002, 88(8): 085503(1−4).

[13] BONAMY D, RAVI-CHANDAR K. Interaction of shear waves and propagating cracks [J]. Phys Rev Lett, 2003, 91(23): 235502(1−4).

[14] XU Qian-gang, ZHANG Hai-feng, HU Zhuang-qi. Wetting behavior of $Fe_{78}B_{13}Si_9$ melt on iron [J]. The Chinese Journal of Nonferrous Metals, 2006, 16(10):1660−1664. (in Chinese)

[15] ARGON A S, SALAMA M. Mechanism of fracture in glassy materials capable of some inelastic deformation [J]. Mater Sci Eng, 1976, 23(22): 219−230.

[16] XI X K, ZHAO D Q, PAN M X, WANG W H, WU Y, LEWANDOWSKI J J. Fracture of brittle metallic glasses: Brittleness or plasticity [J]. Phys Rev Lett, 2005, 94: 125510(1−4).

[17] FAN C, INOUE A. Ductility of bulk nanocrystalline composites and metallic glasses at room temperature [J]. Appl Phys Lett, 2000, 77: 46−68.

**(Edited by LI Xiang-qun)**